Materials Advances

PAPER

Check for updates

A hydrogel transducer for wearable devices: energy supply, electrostatic protection, and circuit modeling

Yue Shi, [ab] Zheming Zhang,[b] Zekun Zhou, [*a] Yao Yao[b] and Jingjie Huang[b]

The application of flexible materials in wearable devices holds great potential. In this paper, a multifunctional integrated hydrogel transducer is developed. It realizes power generation based on the potential difference between copper (Cu) and aluminum (Al) electrodes and the humidity difference of the hydrogel, while it has both humidity sensing and overvoltage protection functions. This device employs a polyacrylamide hydrogel containing NaCl as the conductive medium. By utilizing the potential difference between Cu and Al electrodes, it generates an open-circuit voltage of 0.4–0.6 V, driving ion-directed migration to produce a short-circuit current of 20–40 μA. Experiments show that the short-circuit current increases significantly with ambient humidity, enabling it to sensitively detect changes in air humidity. When used as a load, it exhibits diode characteristics when the voltage is higher than 1.6 V or lower than −0.8 V, effectively limiting the amplitude to protect against static impact. By modeling the equivalent circuit containing the diode, the working mechanism of the device in the energy supply and circuit protection modes is revealed. Compared with the traditional hydrogel transducer, this device realizes the integration of power generation, humidity sensing and limiting protection for the first time. This significantly improves the self-powering and anti-static shock ability of wearable devices in complex environments, providing a new strategy for self-powering and circuit protection of wearable devices.

1. Introduction

With the rapid development of flexible electronics in wearable medical monitoring, smart sensing, and the Internet of Things, miniature energy devices that combine flexibility, safety, and environmental adaptability have emerged as a research hotspot.[1–3] Flexible energy devices need to meet the requirements of mechanical deformation tolerance, biocompatibility, low-power operation, and integration. However, traditional lithium-ion batteries have the risks of electrolyte leakage and rigid structure limitations. Hydrogel has considerable potential for application in wearable devices because of its advantages of high ionic conductivity, mechanical flexibility, and biocompatibility.[4–7]

In recent years, hydrogel-based triboelectric nanogenerators (TENGs),[8,9] ionic thermoelectric generators,[10,11] piezoelectricity-based hydrogel generators,[12–14] and ion mobility-based moisture electrically generated generators (MEGs),[15–17] have made significant progress, and they can be better applied to wearable devices

due to the flexibility of hydrogels, but the electrical output characteristics of these generators are highly dependent on the environment, requiring a stable environment or continuous external stimulation to output a stable voltage and current. On the other hand, hydrogel electrolytes are also developing rapidly in zinc ion batteries (*e.g.*, Zn–MnO$_2$ systems), but they rely on the redox reaction of zinc metal to realize energy storage, and the choice of electrode materials is limited by the prominent problem of dendritic growth.[18,19] Moreover, most hydrogel transducers are only used as a single energy storage element.[20,21]

However, to be used in wearable devices, the effect of human static electricity on the device needs to be considered, especially in the dry winter, where human body static electricity can easily destroy the device.[22] This requires additional protection circuits, whereas there are very few reports on the design of the transducer itself and the integration of the protection circuit function. In addition, since not all hydrogel transducers can be replaced by the voltage source series resistance model, if the hydrogel transducer is to be applied in a more complex circuit system, understanding the equivalent circuit of the device itself is also helpful for the design of the whole system. However, few studies have addressed hydrogel transducer modeling.[23] Overall, existing hydrogels exhibit limited functionality and sensitivity to environmental conditions, and lack electrostatic

[a] *State Key Laboratory of Electronic Thin Films and Integrated Devices, University of Electronic Science and Technology of China, Chengdu, Sichuan 610054, China.*
E-mail: zkzhou@uestc.edu.cn
[b] *College of Communication Engineering, Chengdu University of Information Technology, Chengdu 610225, China*

protection mechanisms. Achieving multifunctionality requires adding additional discrete system components, which inevitably increases the complexity and cost of the entire system. Furthermore, applying hydrogel transducers to other electronic systems becomes significantly more challenging in the absence of equivalent circuit models. This makes equivalent circuit models efficient in complex system applications with reduced design efforts.

With regards to the problems of hydrogel transducers mentioned above, such as single function and lack of equivalent circuit models, this paper presents a hydrogel transducer. It uses hydrogel as the conductive medium with Cu and Al foil tape as the electrodes. This transducer can output a voltage of 0.4–0.6 V and a current of 20–40 μA. Its output voltage is less reliant on the environment. It has a simple structure resistant to mechanical deformation, while possessing the functions of power generation, humidity sensing, and limiting protection. Additionally, this paper models the equivalent circuit of the hydrogel, which is conducive to the subsequent design of some complex circuit systems.

2. Materials and methods

2.1. Materials for the preparation of hydrogels

Acrylamide (AM, ≥99%) was purchased from Sigma-Aldrich. 40 g of AM was dissolved in 100 mL of deionized water (18.2 MΩ cm) to form a 40% (w/v) stock solution; N,N'-methylenebisacrylamide (MBAA, 98%) was purchased from Aladdin Biochemicals and

Technology Co. and stored at 4 °C. The solution was used to formulate a 2% (w/v) crosslinker solution. A 2% (w/v) cross-linker solution was prepared ready-to-use; ammonium persulfate (APS, ≥98%) was purchased from McLean. The 10% (w/v) initiator solution was used; sodium chloride (NaCl, 99.8%) was purchased from Sinopharm Chemical Reagent Co. Deionized water was purified by a Milli-Q system (Millipore, 18.2 MΩ cm).

2.2. Hydrogel preparation process

The precursor solution (20 mL) was prepared as follows: AM monomer, 15% final concentration (w/v) → 15% × 20 mL = 3 g AM (3 g/0.4 = 7.5 mL from the 40% stock solution); MBAA cross-linker, 1.5% by mass of AM → 3 g × 1.5% = 0.045 g → dissolved in 2.25 mL of 2% MBAA stock solution; NaCl, 5 M → 5 mol L^{-1} × 0.02 L × 58.44 g mol^{-1} = 5.844 g; APS initiator, 1% by mass of AM → 3 g × 1% = 0.03 g → dissolved in 0.3 mL of 10% APS solution. NaCl was dissolved in 10 mL of deionized water with magnetic stirring (500 rpm, 10 minutes (min)) and AM stock solution and MBAA solution were added sequentially. The total volume was adjusted to 19.7 mL with deionized water, and then under conditions of 25 °C, high-purity nitrogen gas (99.99%) was passed through the solution in a semi-sealed container for 30 minutes: the nitrogen gas stream displaced and expelled oxygen (along with air), thereby removing dissolved oxygen from the solution.[24] Under nitrogen protection, 0.3 mL of 10% APS solution was injected into the degassed precursor solution, which was then immediately transferred to a pre-coated polytetrafluoroethylene (PTFE) mold (50 mm × 50 mm × 3 mm) treated with a silane
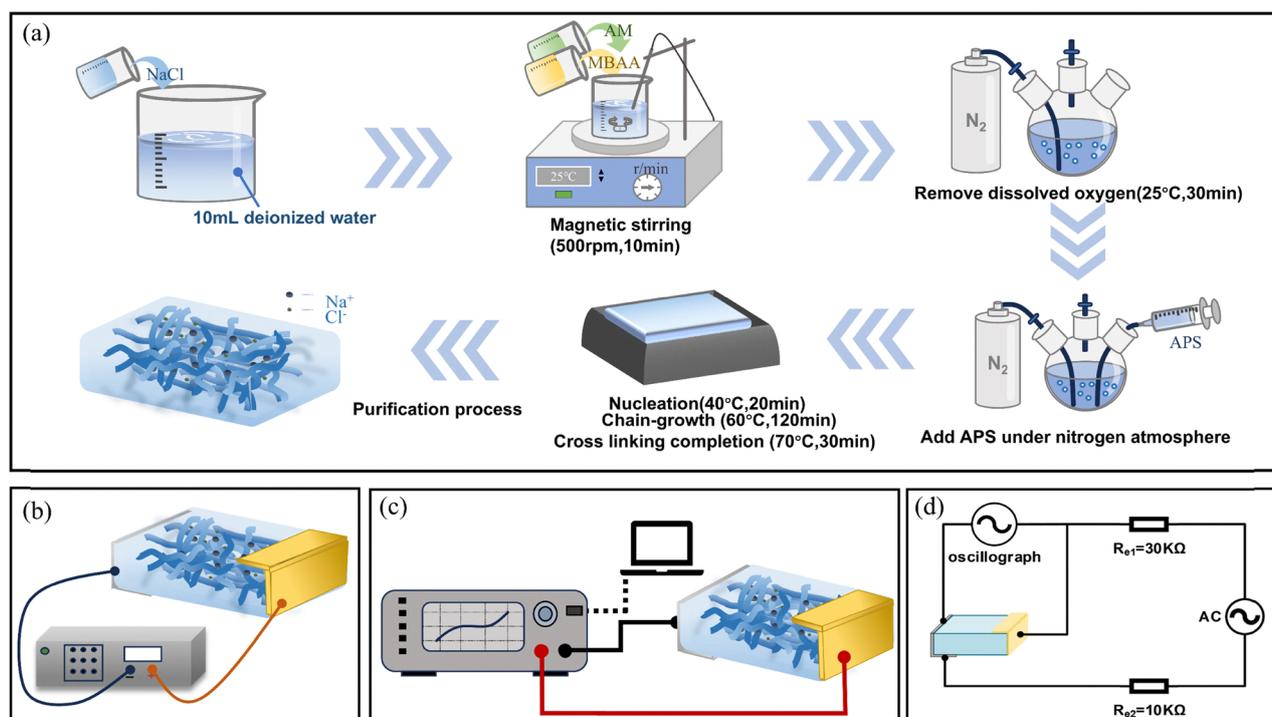

Fig. 1 (a) Flowchart for hydrogel preparation, (b) schematic diagram of hydrogel transducer open-circuit voltage and short-circuit current measurement, (c) schematic diagram of hydrogel transducer $I-V$ characteristic curve scanning, and (d) schematic diagram of hydrogel transducer limiting circuit connection.

release agent for molding; The prepolymerization reaction proceeded at 40 °C for 20 minutes (nucleation stage), followed by main polymerization at 60 °C for 2 hours (chain growth stage). Finally, curing occurred at 70 °C ambient temperature for 30 minutes (crosslinking completion stage). After polymerization, the hydrogel also needs to be purified: the hydrogel was immersed in 200 mL of deionized water for 72 h (changed every 12 h), unreacted monomers were removed and the purity was detected by using a UV-visible spectrophotometer (Jasco V-750) at 280 nm (absorbance <0.05), which completed the preparation of the hydrogel, as shown in Fig. 1a.

2.3. Measurement of open-circuit voltage, short-circuit current and I–V characteristic curve

Cu and Al electrodes were respectively attached to the upper right and lower left corners of the hydrogel. Additionally, wires were connected to one end of the two electrodes, with the Cu electrode serving as the positive electrode and the Al electrode as the negative electrode, as depicted in Fig. 1b. A Keithley 2450 was employed as the measuring instrument, and its positive and negative terminals were respectively connected to the positive and negative terminals of the proposed hydrogel transducer. The open-circuit voltage and short-circuit current of the hydrogel transducer were measured by switching between different gear levels. To obtain the I–V characteristic curve, the Keithley 2450 was used as a voltage source, applying a voltage of -0.2–1.5 V at the positive end of the hydrogel

transducer and continuously scanning the current of the hydrogel transducer, as shown in Fig. 1c.

2.4. Experiments on limiter circuits

GWINSTEK's AFG-2225 serves as the input source for the circuit, inputting a sinusoidal signal with a frequency of 1 Hz. The peak-to-peak value of this sinusoidal signal gradually increases. The GWINSTEK GDS-1104E oscilloscope monitors the circuit, as shown in Fig. 1d. It measures the voltage waveform between the positive and negative electrodes of the designed hydrogel transducer. This observation checks whether a voltage plateau appears across the hydrogel transducer terminals after the input voltage reaches a certain threshold. The presence of such a plateau indicates that the hydrogel transducer exhibits limiting characteristics.

3. Results and discussion

3.1. As an energy source

In this paper, the hydrogel is formed because APS decomposes under heating (within the temperature range of 40–70 °C) to generate sulfate radicals. These sulfate radicals trigger the opening of the double bond of the AM monomer, thereby forming polyacrylamide (PAM) chain radicals. Simultaneously, the double bond of MBAA is attacked by free radicals, and two of its acrylamide groups respectively attach to two different PAM chains to form a covalent cross-linking bond. With the
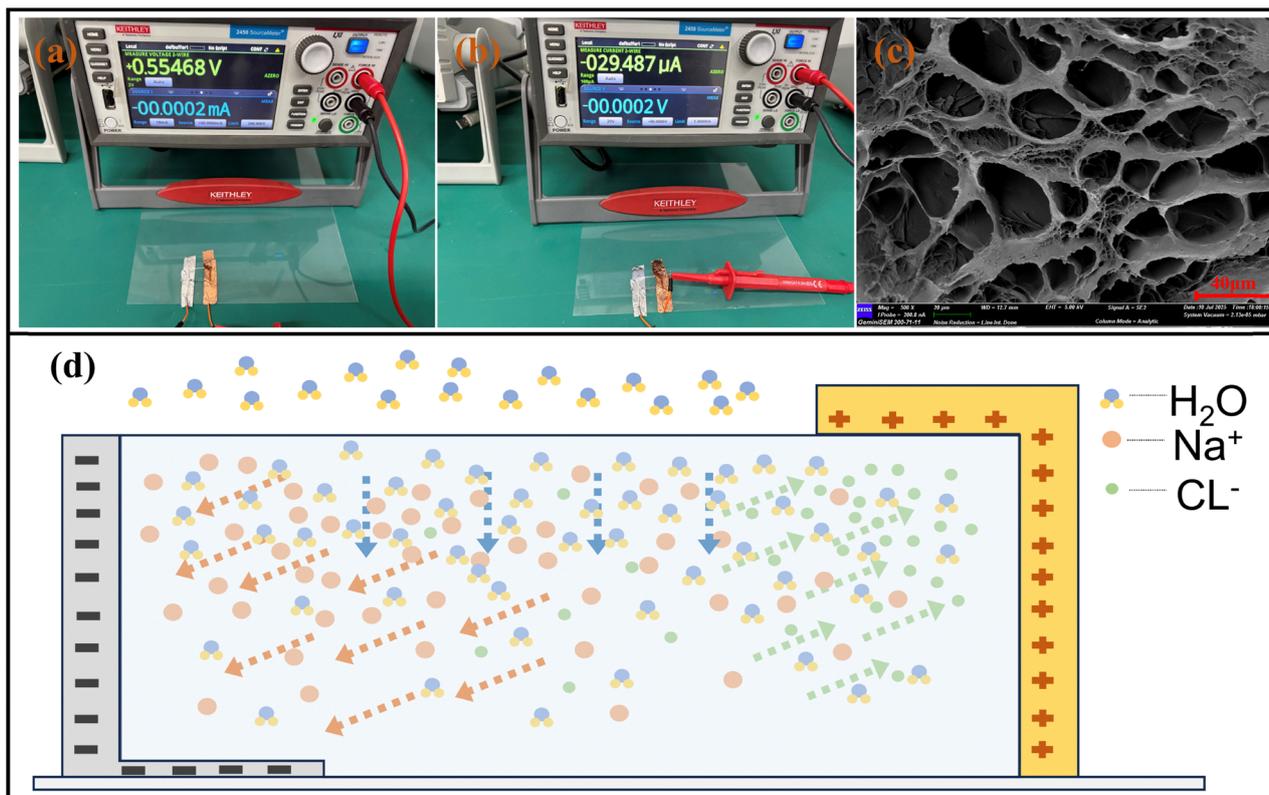

Fig. 2 (a) Open-circuit voltage of a single hydrogel transducer, (b) short-circuit current of a single hydrogel transducer, (c) SEM image of the unitary hydrogel, and (d) schematic diagram of ion movement inside the hydrogel transducer.

completion of the polymerization reaction, a three-dimensional porous network that runs through the aqueous phase of NaCl is ultimately formed inside the hydrogel.[25,26] As shown in Fig. 2a and b, the proposed hydrogel transducer is capable of outputting an open-circuit voltage of 0.4–0.6 V and a short-circuit current of 20–40 μA at room temperature. The micro-view of the hydrogel is observed by using a scanning electron microscope, whose internal structure is shown in Fig. 2c. At the microscopic scale, there are many porous structures that can serve as ion transport channels. As shown in Fig. 2d, since the electrode potential of Cu is higher than that of Al, an electric field exists inside the hydrogel, pointing from Cu to Al. This causes the positive Na^+ ions in the hydrogel to move in the direction of the electric field (*i.e.*, towards the Al pole plate), while the negatively charged Cl^- ions move against the direction of the electric field (*i.e.*, towards the Cu pole plate). In addition, since the bottom of the hydrogel cannot be in contact with air, there is asymmetric moisture absorption between the top and bottom of the hydrogel, resulting in a humidity difference within the hydrogel. This causes water molecules to drive ions to move downward from the top. Due to the presence of an electric field inside the hydrogel, the movement of Cl^- ions driven by water

molecules downward is limited, while the drive for water molecules to promote the downward movement of Na^+ ions is enhanced. Under the combined effect of humidity difference and internal electric field, Na^+ ions form a directional migration from the Cu electrode plate to the Al electrode plate, while Cl^- ions experience a directional migration from the Al electrode plate to the Cu electrode plate, thereby forming a current.

In order to further understand the influence of environment on the power generation ability of the hydrogel transducer, the hydrogel transducer was placed in different air humidity environments and its open-circuit voltage and short-circuit current were measured, and the measurement results are shown in Fig. 3a and b. The experimental results show that the open-circuit voltage of the hydrogel transducer does not change significantly with the elevation of the air humidity, whereas the short-circuit current rises gradually with the elevation of the air humidity. This is because the amide group ($-CONH_2$) on the PAM chain binds to the water molecules through hydrogen bonding, promoting the hydrogel to absorb water and swell.[27,28] As shown in Fig. 3c, swelling causes the expansion of the polymer network, leading to an increase in the spacing of the polymer cross-linking sites and the formation of wider ionic transport
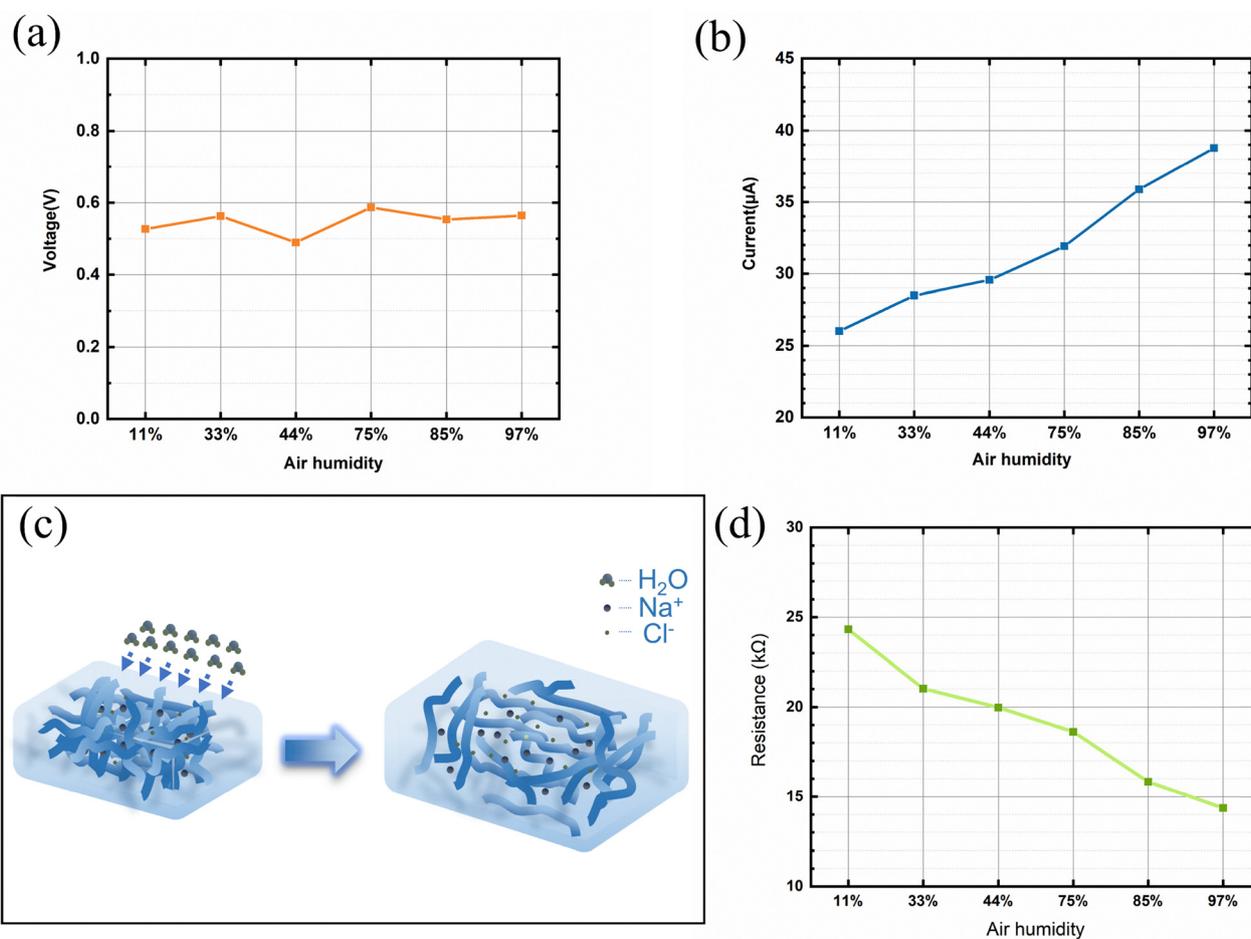

Fig. 3 (a) Variation curves of open-circuit voltage of a single hydrogel transducer under different air humidities, (b) short-circuit current of a single hydrogel transducer in different air humidities, (c) schematic diagram of the expansion of the internal polymer network due to water absorption of the hydrogel, and (d) curve of conductance resistance of the hydrogel transducer with changes in air humidity.

channels, thereby improving the ionic transport efficiency.[29,30] In addition, due to the expansion of the polymer network, the steric hindrance exerted by the polymer chains on the ions is reduced, which further enhances the ion transport rate. Evidently, the increased air humidity causes the hydrogel to absorb water and swell, which in turn boosts the short-circuit current of the hydrogel transducer.[31] As shown in Fig. 3d, the conductance impedance of the hydrogel transducer continuously decreases with increasing air humidity, reflecting changes in the hydrogel's ion transport efficiency.

Based on previous experiments, it can be concluded that the open-circuit voltage of a single hydrogel transducer is 0.4–0.6 V, the short-circuit current is 20–40 μA, and it delivers a maximum output power of 3.5 μW at 11% relative humidity, as shown in Fig. 4a. Although the voltage and current of a single hydrogel transducer are not very high, it is possible to obtain a superposition of the open-circuit voltage and short-circuit current by connecting several hydrogel transducers in series or in parallel as shown in Fig. 4b and c. The series-parallel connection of multiple hydrogel transducers can power many devices, such as light-up diodes, as shown in Video S1. Moreover, hydrogel transducers can be employed to build humidity sensors for detecting environmental humidity. This is based on the property that the current of hydrogel transducers varies in different air humidity. As shown in Video S2, when the surrounding environment's humidity increases due to breathing, the short-circuit current of the hydrogel transducer changes significantly. Consequently, the hydrogel transducer can also be utilized to detect human movement.

3.2. As a load

As shown in Fig. 5a, under the environment of 75% air humidity, the I–V characteristic curve of the hydrogel transducer is obtained by applying a voltage of −0.2–1.5 V to the positive electrode of the hydrogel transducer. It can be noted that when the external voltage is approximately 0.5 V, the slope of the current changes notably. This implies that, compared to hydrogel transducers with an external voltage below 0.5 V, those above 0.5 V experience a significant increase in impedance. Since the internal voltage of the hydrogel transducer is 0.4–0.6 V and it acts as a load simultaneously, the internal and

external voltages of the hydrogel transducer almost cancel each other out, with 0.5 V external voltage, where it is equivalent to the zero-potential point for the two electrode plates. In the case where the external voltage is less than 0.5 V, the current flows in from the Al electrode plate and out from the Cu plate, where Al loses electrons and an oxidation reaction occurs, while Cu gains electrons for a reduction reaction. However, due to the natural conditions, a layer of oxide will form on the surfaces of Cu and Al. Among them, alumina is a dense oxide film,[32,33] as shown in Fig. 5b. Therefore, it is difficult for Al to react with external oxygen to generate alumina, resulting in the thickness of alumina remaining basically unchanged. Because of the Cu oxide being loose and porous, Cu readily undergoes a reduction reaction, leading to the thickness of the Cu oxide decreasing, as shown in Fig. 5c. Consequently, the hydrogel transducer exhibits a small impedance. When the external voltage is greater than 0.5 V, the current direction changes, while Cu loses electrons to be oxidized and Al gains electrons to be reduced. Although the thickness of alumina remains basically unchanged due to its denseness, Cu as the anode will be continuously oxidized to increase oxide thickness at this time, as shown in Fig. 5d, resulting in an increase in the impedance of the hydrogel transducers. To validate the above observations, we examined the thickness of the oxide layer on two identical hydrogel transducers after applying opposite currents for a period of time. As shown in Fig. 5e, after current flowed from the copper electrode to the aluminum electrode for a period, the oxide layer thickness on the copper electrode of the hydrogel transducer was approximately 70 micrometers. Conversely, as depicted in Fig. 5f, after current flowed from the Al electrode to the Cu electrode for a period, the Cu electrode was almost completely oxidized, with an oxide layer thickness exceeding 100 micrometers. This confirms the validity of our viewpoint.

The dielectric strength of alumina is inversely proportional to the thickness of the alumina film.[34] A 380 μm thick alumina has a dielectric strength of up to 31.1–33.2 kV mm^{-1}.[35] In its natural state, the alumina film on an Al electrode is typically 2–10 nm thick. Consequently, the breakdown voltage is higher than 0.332 V. Although the conductivity of Cu oxide is better than that of Al oxide, and there has been no detailed investigation regarding the dielectric strength of Cu oxide, by rough
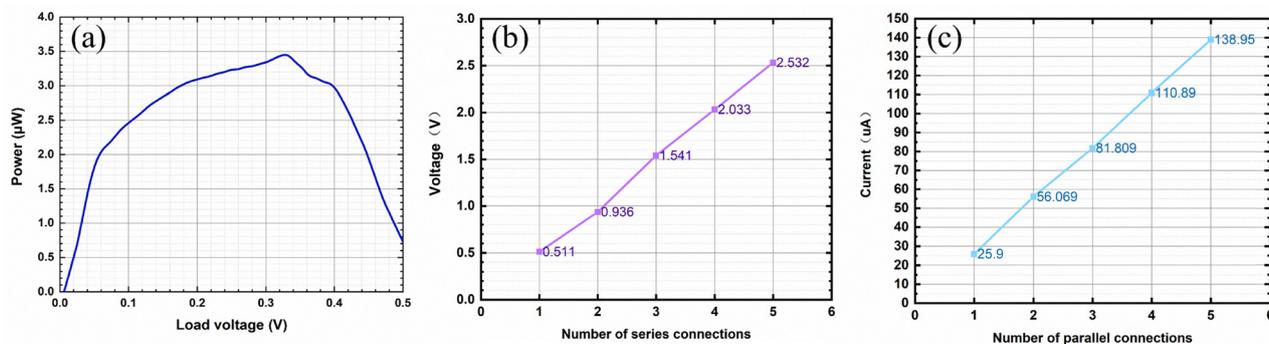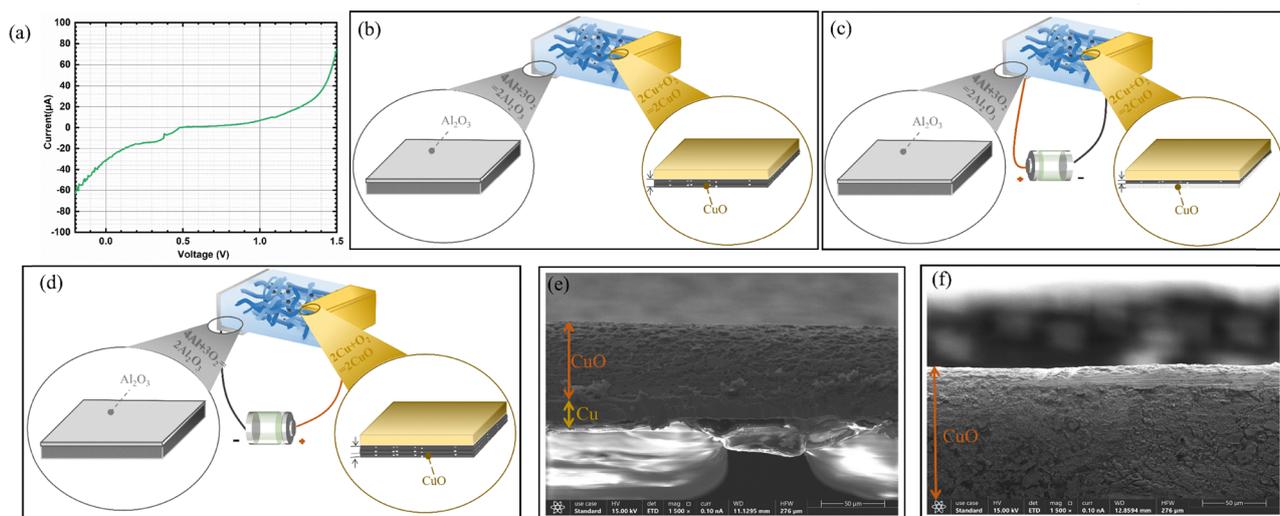

Fig. 4 (a) Power output curve of the hydrogel transducer, (b) series open-circuit voltage variation curve of the hydrogel transducers, and (c) parallel short-circuit current variation curve of the hydrogel transducers.

Fig. 5 (a) $I–V$ characteristic curve of the hydrogel transducer at 75% air humidity, (b) schematic diagram of the oxide film formed by Cu and Al electrode plates in the natural state, (c) schematic diagram of the decrease in thickness of the oxide layer due to the reduction reaction of the Cu electrode plate connected to the negative terminal of the power source, and (d) schematic diagram of the increase in thickness of the oxide layer due to oxidation reaction of the Cu electrode plate connected to the positive terminal of the power source. (e) After applying a current flowing from the Cu electrode to the Al electrode for a period of time across both ends of the hydrogel transducer, the SEM image of the Cu electrode cross-section. (f) After applying a current from the Al electrode to the Cu electrode across the hydrogel transducer for a period of time, a scanning electron microscopy image of the cross-section of the Cu electrode.

estimation, the breakdown voltages of the oxides on the two electrode plates combined should be in the range of a few hundred mV to a few V. As shown in Fig. 5a, when the voltage applied to the hydrogel transducer falls below 0.2 V or rises above 1.2 V, a diode-like $I–V$ characteristic gradually emerges—meaning that once the voltage exceeds a certain threshold, the current surges. This occurs because as the voltage applied between the Cu and Al electrodes gradually increases, the thin oxide layer on the electrode plates is progressively broken down by soft dielectric breakdown.[36] This creates a diode-like effect, causing the current to surge dramatically.

3.3. Verification of diode characterization

From the $I–V$ characteristic curve analysis, it can be obtained that due to the puncturing of the oxide layer on the electrode plate of the proposed hydrogel transducer, a similar diode effect will appear. Therefore, its diode characteristics can be verified through a circuit using the hydrogel transducer. For example, in Fig. 6a, the resistance value of R_{e1} is 30 kΩ and the resistance value of R_{e2} is 10 kΩ. With an increasing input voltage waveform, the voltage waveforms on the proposed hydrogel transducer can be analyzed. As shown in Fig. 6d, V_{AC} is the input voltage waveform of the circuit, V_P is the voltage waveform on the Cu electrode, V_N is the voltage waveform on the Al electrode, and V_M is the voltage waveform of $V_P–V_N$ (*i.e.*, the voltage waveform on the hydrogel transducer). By observing the waveforms, it can be clearly seen that when the peak–peak value of the input voltage is over 4.48 V, there is an apparent limiting effect on the voltage of the proposed hydrogel transducer. From the V_M waveform, it can be observed that when the voltage across the hydrogel transducer is lower than

approximately −0.8 V or higher than 1.6 V, there is a limiting effect on the voltage waveform. Additionally, there is a 0.4 V DC offset, which is attributed to the internal DC voltage of the hydrogel transducer. The voltage limiting characteristics of the proposed hydrogel are due to the soft dielectric breakdown of the oxide films on the Cu electrode and the Al electrode. If the input voltage continues to increase, as shown in Fig. 6e, the voltage waveform of the hydrogel transducer basically does not change due to its diode characteristics. It can be seen that the oxide film on the electrode plate of the hydrogel transducer, as analyzed from the $I–V$ characteristic curve in the previous section, will be broken down after applying a certain voltage, thereby exhibiting diode characteristics. This demonstrates that the proposed hydrogel transducer can not only be used as an energy source or humidity sensor, but also can serve as a protection circuit by utilizing its limiting characteristics.

3.4. Equivalent modeling

Through the above analysis, the following characteristics of the hydrogel transducer can be concluded: firstly, its open-circuit voltage is 0.4–0.6 V, and the short-circuit current is 20–40 μA. Secondly, the internal resistance of the hydrogel transducer varies with the direction of current. Lastly, when the voltage difference between the Cu electrodes and the Al electrodes is lower than −0.8 V or higher than 1.6 V, the hydrogel transducer exhibits diode characteristics with a limiting effect. Therefore, the equivalent circuit model of the hydrogel transducer can be derived as shown in Fig. 6b and c, where D_0, D_1, and D_2 are diodes, D_0 is an ideal diode, the conduction voltages of D_1 and D_2 are 1.2 V, V_{source} is the 0.4–0.6 V internal energy source of the hydrogel transducer, and based on the open-circuit voltage and
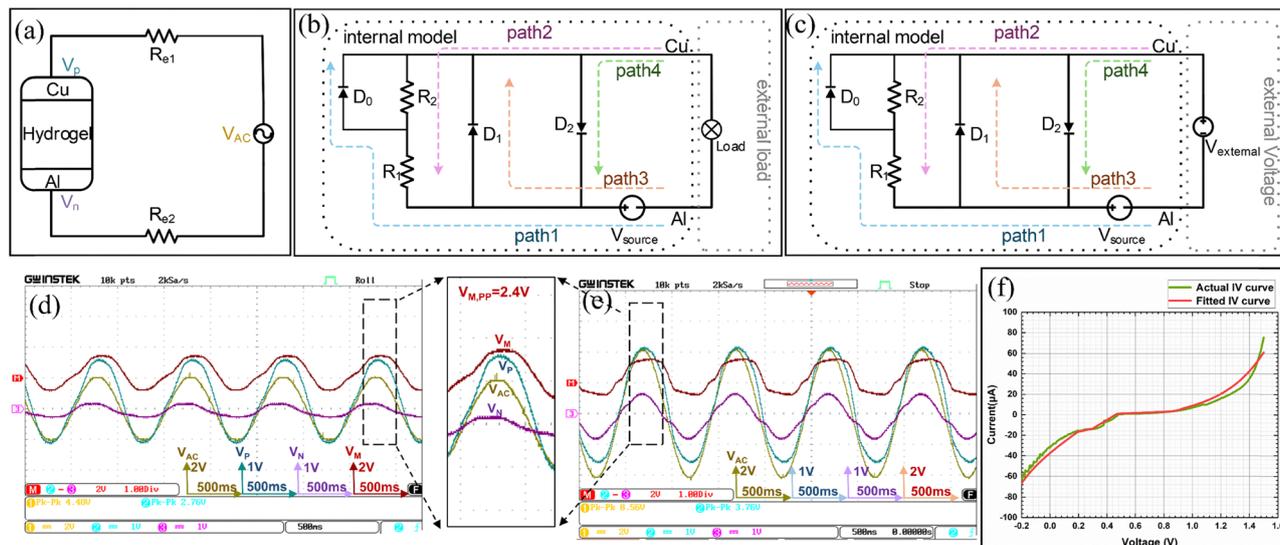
Fig. 6 (a) Hydrogel transducer limiting circuit diagram, (b) equivalent circuit diagram when the hydrogel transducer is used as an energy source to supply power to a load, (c) equivalent circuit diagram when the hydrogel transducer is used as a load, (d) voltage waveforms of the hydrogel transducer limiting circuit when the input sinusoidal voltage peak-to-peak value is 4.48 V, (e) voltage waveforms of the hydrogel transducer limiting circuit when the input sinusoidal voltage peak-to-peak value is 8.56 V, and (f) comparison of the actual IV characteristic curve of the hydrogel transducer and the fitted IV characteristic curve from the equivalent circuit model.

Table 1 Performance comparison of the hydrogel transducer developed in this paper with other transducers

Parameter	Ref. 2	Ref. 3	Ref. 5	Ref. 13	Ref. 14	Ref. 15	Ref. 18	Ref. 19	This work
Voltage (V)	0.55	0.24	0.164	0.16	0.88	0.34	0.31	0.34	0.6
Current (μA)	3.28	16.1	—	—	11.2	1	23	33.23	40
Power density (μW cm^{-2})	0.146	0.965	—	0.004	1.36	0.085	1.782	2.824	6
Multifunctional	No	No	No	No	No	No	No	No	Yes
Circuit model	No	No	No	No	No	No	No	No	Yes

the short-circuit current of the hydrogel transducer, the resistance value of R_1 can be estimated to be about 13.3–30 kΩ. When the hydrogel transducer is used as an energy source, the current in the model flows through path1 to supply power to the external circuit as shown in Fig. 6b. When the hydrogel transducer is used as a load, four cases need to be analyzed as shown in Fig. 6c. $V_{external}$ is the external voltage connected to the hydrogel transducer, when $V_{external} < -0.8$ V, D_1 turns on, path3 conducts, path1 is shorted, and the voltage across the hydrogel transducer is limited to -0.8 V; when -0.8 V $< V_{external} < 0.4$ V, path1 conducts; when 0.4 V $< V_{external} < 1.6$ V, the current direction changes, D_0 cuts off, path2 conducts, and the internal resistance of the hydrogel transducer increases; when $V_{external} > 1.6$ V, path4 conducts, path2 is shorted, and the voltage across the hydrogel is limited to 1.6 V. As shown in Fig. 6f, comparing the IV characteristic curve simulated from the equivalent circuit diagram with the actual IV characteristic curve of the hydrogel transducer is sufficient to validate the accuracy of the equivalent circuit diagram, only with some minor discrepancies.

Table 1 presents a performance comparison between the hydrogel transducer developed in this study and other similar transducers. It can be observed that the transducer developed

in this study achieves high output power density while integrating an energy source, humidity sensor, and electrostatic protection. Furthermore, the modeling of the equivalent circuit for this transducer provides valuable insights for its subsequent application in complex circuit systems.

4. Conclusions

In this study, a multifunctional integrated device based on Cu–Al electrodes and NaCl–doped polyacrylamide hydrogel is developed. For the first time, it realizes the integrated design of power generation, humidity sensing, and limiting protection functions. Experiments indicate that at room temperature, the hydrogel transducers can stably output an open-circuit voltage of 0.4–0.6 V with a short-circuit current of 20–40 μA. The short-circuit current increases significantly with ambient humidity, and the sensitivity can be used for detecting breathing. When used as a load, the device exhibits diode characteristics when an external voltage is applied below -0.8 V or above 1.6 V, and provides electrostatic surge protection by soft dielectric breakdown of the electrode oxide layer. Based on the equivalent circuit model, the dynamic operating mechanism of the device

in energy supply and protection modes is revealed. Compared with traditional hydrogel transducers, this design breaks through the single-function limitation and provides an integrated solution for self-powering and circuit protection of wearable devices.

Future research may enhance voltage-limiting accuracy by optimizing electrode materials (such as precious metal alloys) and further validate the model's universality in transient circuits, thereby advancing its application in wearable devices and energy harvesting systems.

Author contributions

Yue Shi: methodology, investigation, data curation, formal analysis, validation, visualisation, writing – original draft, and writing – review and editing. Zheming Zhang: methodology, formal analysis and validation. Zekun Zhou: conceptualisation, funding acquisition, resources, project administration, supervision, writing – review and editing. Yao Yao: formal analysis. Jingjie Huang: formal analysis.

Conflicts of interest

There are no conflicts to declare.

Data availability

The data that supports the findings of this study are available from the corresponding authors upon reasonable request.

Supplementary information (SI) is available. See DOI: https://doi.org/10.1039/d5ma01161b.

Acknowledgements

Notes and references

1 Y. Luo, M. Wang, C. Wan, P. Cai, X. J. Loh and X. Chen, *Adv. Mater.*, 2020, **32**, 2001903.

2 J. Zhang, J. Zhuang, L. Lei and Y. Hou, *J. Mater. Chem. A*, 2023, **11**, 3546–3555.

3 A. Guchait, S. Pramanik, D. K. Goswami, S. Chattopadhyay and T. Mondal, *ACS Appl. Mater. Interfaces*, 2024, **16**, 46844–46857.

4 T. Dutta, P. Chaturvedi, I. Llamas-Garro, J. S. Velázquez-González, R. Dubey and S. K. Mishra, *RSC Adv.*, 2024, **14**, 12984–13004.

5 P. He, R. Guo, K. Hu, K. Liu, S. Lin, H. Wu, L. Huang, L. Chen and Y. Ni, *Chem. Eng. J.*, 2021, **414**, 128726.

6 N. Liu, H. Ma, M. Li, R. Qin and P. Li, *FlexMat*, 2024, **1**, 269–301.

7 B. Wu, K. Li, L. Wang, K. Yin, M. Nie and L. Sun, *FlexMat*, 2025, **2**, 55–81.

8 Z. Shi, Y. Zhang, J. Gu, B. Liu, H. Fu, H. Liang and J. Ji, *Sensors*, 2024, **24**, 4298.

9 X. Pu, M. Liu, X. Chen, J. Sun, C. Du, Y. Zhang, J. Zhai, W. Hu and Z. L. Wang, *Sci. Adv.*, 2017, **3**, e1700015.

10 Z. Wang, N. Li, Z. Zhang, X. Cui and H. Zhang, *Nanoenergy Adv.*, 2023, **3**, 315–342.

11 C.-G. Han, X. Qian, Q. Li, B. Deng, Y. Zhu, Z. Han, W. Zhang, W. Wang, S.-P. Feng, G. Chen and W. Liu, *Science*, 2020, **368**, 1091–1098.

12 R. Chen, T. Zou, B. Zhang, Z. Yang, Y. Wang, P. Yu, H. Cheng, J. Zhao, X. Liu, X. Yang, L. Wang, Y. Li and Y. Cheng, *Int. J. Biol. Macromol.*, 2025, **285**, 138287.

13 Y. Shi, Y. Guan, M. Liu, X. Kang, Y. Tian, W. Deng, P. Yu, C. Ning, L. Zhou, R. Fu and G. Tan, *ACS Nano*, 2024, **18**, 3720–3732.

14 Y. Song, R. Zhang, M. Qu, R. Zheng, Q. Zhao, P. Tang, Y. Bin and H. Wang, *React. Funct. Polym.*, 2024, **195**, 105806.

15 J. Pei, G. Chen, Z. Li, Z. Zhou, A. Chen, S. Xie and X. Jiang, *Ind. Eng. Chem. Res.*, 2023, **62**, 21666–21672.

16 Y. Han, Y. Wang, M. Wang, Z. Lv, Z. Zhang and H. He, *Chem. Commun.*, 2024, **60**, 6178–6181.

17 C. Xu, C. Fu, Z. Jiang, T. Yang and M. Xin, *ACS Appl. Nano Mater.*, 2023, **6**, 5930–5938.

18 M. A. Elkodous, H. A. Hamad, M. I. A. A. Maksoud, G. A. M. Ali, M. E. Abboubi, A. G. Bedir, A. A. Eldeeb, A. A. Ayed, Z. Gargar, F. S. Zaki, D. A. M. Farage, A. Matsuda, M. R. Abdelnour, B. A. Sabra, A. Elsayed, T. A. Abdelrazek, S. T. Abdelhameed, M. A. Gharieb, M. M. Rabee, S. A. Aboeldiar, N. A. Abdo, A. M. Elwakeel, A. S. Mahmoud, M. M. M. Elsaid, W. M. Omar, R. A. Hania, N. G. Mahmoud, A. S. S. Elsayed, T. M. Mohamed, M. A. Sewidan, M. A. M. Sayed, A. A. Abbas, A. H. Elsayed, A. M. Alazab, M. A. Basyooni, M. Magdy, E. A. Mashaly, O. M. Salem, S. Saber, A. A. Hafez, W. K. Tan and G. Kawamura, *Nanotechnol. Rev.*, 2022, **11**, 2215–2294.

19 J. Cho, G. G. Yadav, M. Weiner, J. Huang, A. Upreti, X. Wei, R. Yakobov, B. E. Hawkins, M. Nyce, T. N. Lambert, N. S. Bell, N. B. Schorr, M. N. Booth, D. E. Turney, G. Cowles and S. Banerjee, *Polymers*, 2022, **14**, 417.

20 L. Guo, Y.-B. Liu, W.-X. Li, J.-Y. Gong, W. Zuo, Y.-L. Liu and P. Fu, *ACS Appl. Nano Mater.*, 2024, **7**, 20913–20919.

21 G. Ma, W. Li, X. Zhou, X. Wang, M. Cao, W. Ma, J. Wang, H. Yu, S. Li and Y. Chen, *ACS Appl. Polym. Mater.*, 2024, **6**, 7066–7076.

22 Z. Pan, X. Li, W. Hao, R. Miao and A. Wang, *IEEE J. Electron Devices Soc.*, 2023, **11**, 700–707.

23 G. Ciarleglio, E. Toto and M. G. Santonicola, *Polymers*, 2023, **15**, 1022.

24 H. Chen, J. Yang, Z. Liu, Y. Li, Z. Tang, X. Shi and Q. Chen, *Adv. Funct. Mater.*, 2025, **35**, 2413171.

25 Y. Zheng, Y. Wang, T. Nakajima and J. P. Gong, *ACS Macro Lett.*, 2024, **13**, 130–137.

26 S. Ronken, D. Wirz, A. U. Daniels, T. Kurokawa, J. P. Gong and M. P. Arnold, *Biomech. Model. Mechanobiol.*, 2013, **12**, 243–248.

27 L. Cacopardo, N. Guazzelli, R. Nossa, G. Mattei and A. Ahluwalia, *J. Mech. Behav. Biomed. Mater.*, 2019, **89**, 162–167.

28 H. J. Zhang, T. L. Sun, A. K. Zhang, Y. Ikura, T. Nakajima, T. Nonoyama, T. Kurokawa, O. Ito, H. Ishitobi and J. P. Gong, *Adv. Mater.*, 2016, **28**, 4884–4890.

29 S. Zhao, Y. Zuo, T. Liu, S. Zhai, Y. Dai, Z. Guo, Y. Wang, Q. He, L. Xia, C. Zhi, J. Bae, K. Wang and M. Ni, *Adv. Energy Mater.*, 2021, **11**, 2101749.

30 P. Yang, C. Feng, Y. Liu, T. Cheng, X. Yang, H. Liu, K. Liu and H. J. Fan, *Adv. Energy Mater.*, 2020, **10**, 2002898.

31 D. Stein, M. Kruithof and C. Dekker, *Phys. Rev. Lett.*, 2004, **93**, 035901.

32 G. Saito, S. Hosokai, M. Tsubota and T. Akiyama, *J. Appl. Phys.*, 2011, **110**, 023302.

33 W. Ota, Y. Kojima, S. Hosokawa, K. Teramura, T. Tanaka and T. Sato, *Phys. Chem. Chem. Phys.*, 2021, **23**, 2575–2585.

34 N. E. Korobova, M. S. Batalova and B. E. Alpysbayeva, *J. Phys.: Conf. Ser.*, 2021, **1954**, 012021.

35 B. Mieller, *J. Adv. Ceram.*, 2019, **8**, 247–255.

36 K. Fujiwara, T. Nemoto, M. J. Rozenberg, Y. Nakamura and H. Takagi, *Jpn. J. Appl. Phys.*, 2008, **47**, 6266.